IEEE Access
Multidisciplinary | Rapid Review | Open Access Journal

Date of publication xxxx 00, 0000, date of current version xxxx 00, 0000.

Digital Object Identifier 10.1109/ACCESS.2017.DOI

Plasma-Based Reflecting and Transmitting Surfaces

M. MAGAROTTO, (MEMBER, IEEE)[1,2], L. SCHENATO, (MEMBER, IEEE)[1,2], M. SANTAGIUSTINA, (MEMBER, IEEE)[1,2], A. GALTAROSSA, (FELLOW, IEEE)[1,2], A.-D. CAPOBIANCO, (MEMBER, IEEE)[1,2]

[1]Department of Information Engineering, University of Padova, Padova, IT
[2]CNIT - National Inter-University Consortium for Telecommunications, Parma, IT

Corresponding author: M. Magarotto (e-mail: mirko.magarotto@unipd.it).

ABSTRACT A theoretical model is proposed to preliminary assess the performance of plasma-based reflecting and transmitting surfaces. The model has been verified and, subsequently, exploited in a feasibility study to implement beam steering and polarization control. Theoretical findings laid the basis for the numerical design of a reconfigurable plasma-aided horn antenna. Notably, the solution proposed is capable of both beam steering and polarization control relying on a plasma-based transmitting surface. Specifically, the main lobe can be steered in the range $0^\circ - 50^\circ$ maintaining the gain > 10 dBi, the relative side lobe level < -10 dB, and the reflection coefficient < -10 dB. The bandwidth is 1 GHz for an operation frequency of 10 GHz. Polarization conversion is feasible maintaining values of the plasma parameters and magnetic induction field compatible with the technology at the state of the art.

INDEX TERMS Gaseous Plasma Antenna, Horn Antenna, Beam Steering, Polarisation Conversion.

I. INTRODUCTION

GASEOUS Plasma Antennas (GPAs) are devices in which an ionized gas, namely plasma, is used to transmit and receive electromagnetic (EM) signals [1]. GPAs offer several advantages over metallic antennas [2]. First, it is possible to reconfigure the antenna performance (e.g., radiation pattern and operation frequency) by electronically controlling the plasma properties (e.g., density) [3], [4]. Second, when the plasma is switched off, the antenna almost stops interacting with the EM signal [5]. Thus, GPAs are particularly suitable to form arrays or to be applied in scenarios where stealth is required [6], [7]. Third, the EM response of a GPA is frequency dependent; thus, antennas with different operation frequencies can be stacked together [8].

Among GPAs, plasma-based reflecting surfaces are particularly suitable to implement beam steering [9], polarization control [10], and to combine these two features [11]. Numerical designs have been proposed to implement plasma-based reflecting surfaces via Cold Cathode Fluorescence Lamps (CCFL), which is a plasma production technology at the state of the art [12], [13]. At the same time, plasma-based transmitting surfaces are put forward to enable beam steering operations [14]–[16] or polarization control [17]. The possibility to exploit plasma discharges in a transmitarray [18], [19] or a plasma lens [20] has been investigated too.

The scope of the present paper is twofold. First, a theoretical model is proposed to assess the feasibility of a reconfigurable plasma-based transmitting and reflecting surface. Second, the numerical design of a plasma-aided horn antenna is presented. The latter relies on a reconfigurable plasma-based transmitting surface placed in front of a metallic horn antenna. Theoretical models to handle the propagation of EM waves through a plasma slab are available for both reflecting [9], [10] and transmitting [21], [22] surfaces. The novelty of the proposed approach lies in the adoption of the formalism of ABCD matrices [23] to quickly evaluate the performance of both reflecting and transmitting surfaces in terms of beam steering and polarization control. Regarding the plasma-aided horn antenna, this is the first design ever proposed that enables both beam steering and polarization control via a plasma-based transmitting surface. Similar features have been demonstrated relying on conventional metasurfaces [24]–[27] but never in the framework of GPAs.

II. METHODOLOGY

The relative permittivity of plasma ε_{pl} is a tensor that accounts for the anisotropy triggered by a magnetic induction field $\mathbf{B}_0$ [28]. It is convenient to express ε_{pl} in a Cartesian

reference frame where the z-axis is aligned with $\mathbf{B}_0$,

$$\varepsilon_{pl} = \begin{pmatrix} S & -\jmath D & 0 \\ \jmath D & S & 0 \\ 0 & 0 & P \end{pmatrix} . \tag{1}$$

The adimensional parameters S, D, and P read [28]

$$S = 1 - \frac{XU}{U^2 - Y^2} , \quad D = -\frac{XY}{U^2 - Y^2} , \quad P = 1 - \frac{X}{U} , \tag{2}$$

where the coefficients X, Y, and U are strictly related to the plasma properties. The following relations apply [28]

$$X = \frac{\omega_p^2}{\omega^2} , \qquad Y = \frac{\omega_c}{\omega} , \qquad U = 1 + \jmath\frac{\nu}{\omega} , \tag{3}$$

where ω_p is the plasma frequency, ω_c the cyclotron frequency, ν the collision frequency, and ω the wave frequency. Notably, ω_p, ω_c, and ν are driven by macroscopic plasma parameters [28]

$$\omega_p = \sqrt{\frac{q^2 n_e}{m\varepsilon_0}} , \qquad \omega_c = \frac{qB_0}{m} , \qquad \nu = n_0 K(T_e) , \tag{4}$$

where q is the elementary charge, m the electron mass, ε_0 the vacuum permittivity, n_e the plasma density, B_0 the intensity of the magnetic induction, n_0 the neutral density, and K a rate constant which depends on the electrons' temperature T_e. Specifically, ω_p depends on n_e, which, in practice, can be controlled by varying the electrical power used to sustain the plasma discharge. Similarly, ω_c depends on B_0, which can be reconfigured relying on electromagnets. The parameter ν is associated with Ohmic losses and has a major dependence on n_0, which, according to the plasma discharges at the state of the art [29], is related to the maximum value of n_e required.

The following dispersion relation describes the wave propagation in plasma [28]

$$u^2 = 1 - \frac{X}{Q} , \tag{5}$$

where u is the index of refraction and the adimensional parameter Q reads

$$Q = U - \frac{Y^2 \sin^2\theta}{2(U-X)} \pm \left[\frac{Y^4 \sin^4\theta}{4(U-X)^2} + Y^2 \cos^2\theta \right]^{0.5} . \tag{6}$$

The angle θ forms between the vector $\mathbf{B}_0$ and the direction in which the EM waves propagate. Eq. 5 has two solutions: u_+ and u_-, respectively (the notation refers to the sign adopted in Eq. 6). Namely, two wave modes characterized by the index of refraction u_+ and u_- coexist in a magnetized plasma [10]. This holds unless $B_0 = 0$, since an unmagnetized plasma is an isotropic material in which just one degenerate wave mode, associated with the index of refraction u, propagates [9].

Wave modes are propagative if their index of refraction is almost real [10]. This occurs in an unmagnetized plasma if $n_e \leq n_e^p$, where n_e^p identifies the value of plasma density for which the wave frequency equals ω_p [9]. On the other hand, if $B_0 \neq 0$, intervals of propagation are delimited by the thresholds n_e^R, n_e^0, n_e^p, and n_e^L [10]. These values of plasma density trigger specific resonances or cut-offs [28]. For example, the condition $n_e > n_e^L$ in a magnetized plasma implies that EM waves are evanescent [10].

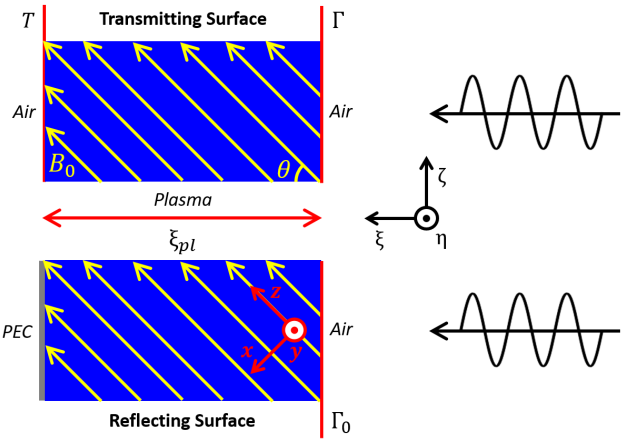

FIGURE 1. Schematic of the transmitting and reflecting surfaces described by the theoretical model.

A. THEORETICAL MODEL

A theoretical model is proposed to evaluate the feasibility of plasma-based transmitting and reflecting surfaces. Unlike other approaches proposed in the literature [9], [10], the current model relies on the formalism of ABCD matrices [23], which allows treating configurations both in transmission and reflection. A plane wave propagating along the ξ-axis (see Fig. 1) is assumed to impinge normally on a uniform plasma slab of thickness ξ_{pl}. Both magnetized and non-magnetized plasmas can be handled. If present, the magnetic induction field $\boldsymbol{B}_0$, aligned with the z-axis, forms an angle θ with the ξ-axis and, in turn, with the direction of propagation of the plane wave. In a transmitting configuration, air extends to the infinite on both sides of the plasma slab. The transmitted and reflected fields read

$$\mathbf{E}_t = T\mathbf{E}_i , \tag{7a}$$

$$\mathbf{E}_r = \Gamma\mathbf{E}_i , \tag{7b}$$

where $\mathbf{E}_i$, $\mathbf{E}_t$, and $\mathbf{E}_r$ are the complex vectors that describe the incident, transmitted, and reflected fields, respectively. T is the transmission coefficient evaluated at the second air-plasma interface, while Γ is the reflection coefficient at the first air-plasma interface (see Fig. 1). On the other hand, in a reflecting configuration, the plasma slab is assumed to be placed on top of an infinite ground plane made from a Perfect Electric Conductor (PEC). The reflected field reads

$$\mathbf{E}_r = \Gamma_0\mathbf{E}_i , \tag{8}$$

where Γ_0 is the reflection coefficient at the air-plasma interface (see Fig. 1).

The coefficients T, Γ, and Γ_0 can be computed according to the formalism of the ABCD matrices. The components of the ABCD matrix associated to the plasma slab read [23]

$$A = \cos\left(2\pi u \frac{\xi_{pl}}{\lambda}\right), \tag{9a}$$

$$B = -j\frac{Z_0}{u}\sin\left(2\pi u \frac{\xi_{pl}}{\lambda}\right), \tag{9b}$$

$$C = -j\frac{u}{Z_0}\sin\left(2\pi u \frac{\xi_{pl}}{\lambda}\right), \tag{9c}$$

$$D = \cos\left(2\pi u \frac{\xi_{pl}}{\lambda}\right), \tag{9d}$$

where λ is the wavelength in air and Z_0 is the intrinsic impedance of vacuum. In case of a transmitting surface, the coefficients T and Γ read [23]

$$T = \frac{2}{A + B/Z_0 + CZ_0 + D}, \tag{10a}$$

$$\Gamma = \frac{A + B/Z_0 - CZ_0 - D}{A + B/Z_0 + CZ_0 + D}. \tag{10b}$$

While, for a reflecting surface, Γ_0 reads [23]

$$\Gamma_0 = \Gamma - \frac{T^2}{1+\Gamma}, \tag{11}$$

where T and Γ are computed according to Eq. 10.

It is worth specifying that, to avoid a cumbersome notation, the relations presented in this section apply to each wave mode, namely, they hold straightforwardly for a non-magnetized plasma. General results can be easily obtained by combining the contributions of multiple wave modes according to the procedure described in [10]. At the same time, the proposed model holds if the intensity of the signal is not high enough to affect plasma properties. Considering the technology at the state of the art [29], this condition applies if the signal power is less than several Watts [3].

Finally, once $\mathbf{E}_r$ and $\mathbf{E}_t$ are known, the capability of a plasma surface to exploit polarization conversion is quantified in terms of Polarization Conversion Ratio (PCR) and Axial Ratio (AR) [10], [11]. The former describes the cross-polarization conversion while the latter conventionally defines a circularly polarized signal if AR $<$ 3 dB [30].

B. NUMERICAL MODEL

Numerical simulations are performed with the commercial software CST Studio Suite ®. Analyses are accomplished to verify the theoretical model and to preliminary design a reconfigurable plasma-aided horn antenna. The former simulations aim at reproducing the plasma slab depicted in Fig. 1. Thus, a rectangular plasma block of thickness ξ_{pl} is analysed assuming Floquet boundary conditions along the η-axis and ζ-axis while open boundary conditions are imposed along the direction of propagation of the plane wave (i.e., the ξ-axis) [9]–[11]. The horn antenna is simulated assuming open boundary conditions in all directions. An exhaustive description of the antenna design is reported in section IV.

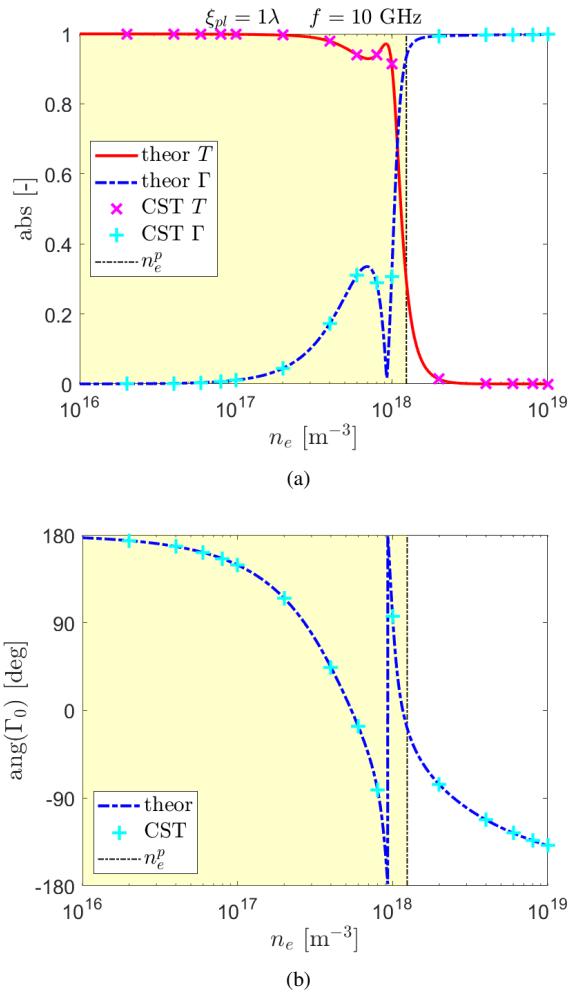

FIGURE 2. Comparison between theoretical model (theor) and numerical results (CST). (a) Transmitting surface, the amplitude of the transmission (T) and reflection (Γ) coefficients. (b) Reflecting surface, phase of the reflection coefficient (Γ_0). The colored background indicates the interval in which waves propagate in plasma, $\nu = 3.1 \times 10^8$ Hz.

III. THEORETICAL RESULTS

The theoretical model has been verified against numerical results to assess its reliability. Subsequently, it has been exploited to compare the performance of plasma-based transmitting and reflecting surfaces.

A. VERIFICATION

The theoretical model has been verified against numerical results in the case of both non-magnetized and magnetized plasmas (see Fig. 2 and Fig. 3, respectively). Given a wave frequency $f = 10$ GHz, a non-magnetized plasma slab of thickness $\xi_{pl} = \lambda = 30$ mm is considered. A plane wave linearly polarized along the η-axis is assumed to impinge on the slab. Comparison against numerical results is reported in terms of the amplitude of the T and Γ coefficients, which describe a transmitting surface (see Fig. 2(a)), and phase of Γ_0, which is associated with a reflecting surface (see Fig. 2(b)). Results show a good agreement between theo-

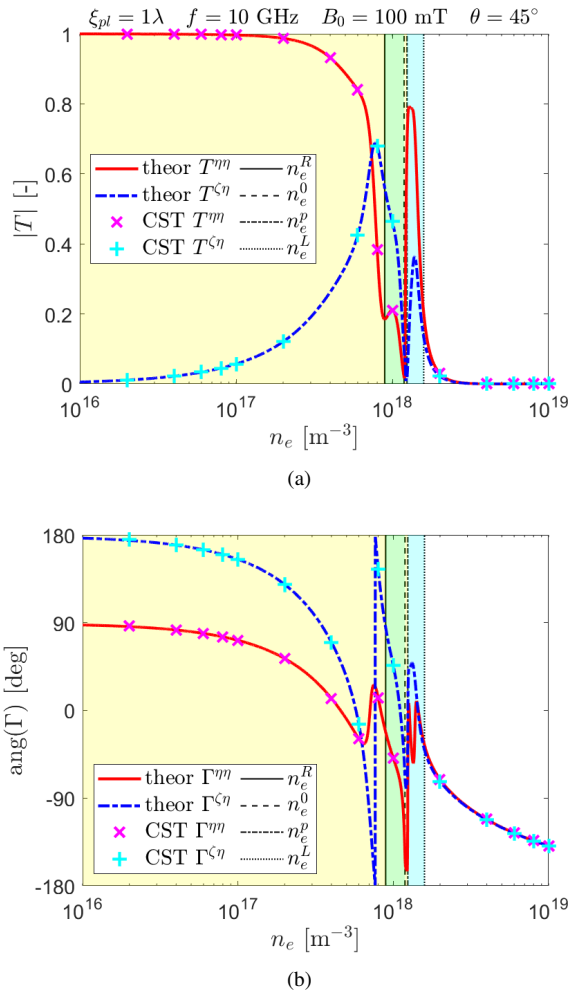

FIGURE 3. Comparison between theoretical model (theor) and numerical results (CST). Magnetized transmitting surface: (a) amplitude of the transmission coefficient (T), and (b) phase of the reflection coefficient (Γ) expressed by components. The colored background indicates the interval in which waves propagate in plasma, $\nu = 3.1 \times 10^8$ Hz.

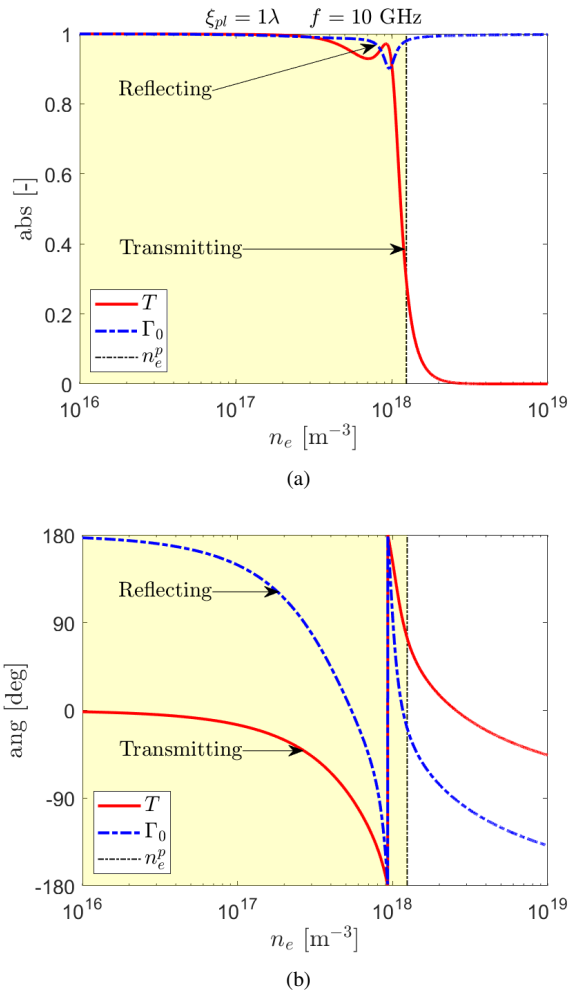

FIGURE 4. Comparison between a transmitting and reflecting surface in terms of (a) amplitude, and (b) phase of the transmission (T) and reflection (Γ_0) coefficients. The colored background indicates the interval in which waves propagate in plasma, $\nu = 3.1 \times 10^8$ Hz.

retical and numerical results, with differences within 1%. The same slab is adopted to verify the theoretical model in the case of a magnetized plasma with $B_0 = 100$ mT, and $\theta = 45°$. The amplitude of T and the phase of Γ, associated with a transmitting surface, are depicted in Fig. 3. Provided the capability of a magnetized plasma to affect polarization, it is necessary to refer T and Γ to the η and ζ components of the transmitted and reflected fields, respectively. For example, $T^{\zeta\eta}$ indicates the ratio between the ζ component of $\boldsymbol{E}_t$ and the η component of $\boldsymbol{E}_i$. Also, in this case, theoretical results match well the numerical ones, with minor differences within 1%. This confirms the reliability of the proposed model.

B. TRANSMITTING AND REFLECTING SURFACES

The theoretical model has been exploited to compare the performance of a plasma-based surface either in transmitting or reflecting mode, with the aim to assess the pros and cons of the two configurations. A non-magnetized plasma slab of thickness $\xi_{pl} = \lambda = 30$ mm ($f = 10$ GHz) is analysed in transmitting and reflecting configuration in Fig. 4. Consistently with the literature [9], the amplitude of the reflection coefficient Γ_0 is close to the unit for each value of n_e considered. This is associated with a mild Ohmic loss occurring in the plasma medium [9]. On the other hand, in the transmitting configuration T drops for $n_e > n_e^p$ which is consistent with the absence of waves propagating for this range of densities. This aspect imposes a limit on the possibility of steering a transmitted signal. Indeed, even if its phase can be reconfigured over 360° varying n_e, only in the range $n_e \leq n_e^p$ the intensity of the transmitted signal is non-negligible. In the analyzed configuration, the phase of T can be controlled over approximately 180° if $|T| \approx 1$ is required. This limitation can be overcome by enlarging ξ_{pl}, in fact, the phase of Γ_0 varies more rapidly than for T given that the path travelled by a wave in a reflecting configuration is doubled with respect to the equivalent transmitting configuration. The theoretical model predicts a value of $\xi_{pl} \approx 2\lambda$ to guarantee a

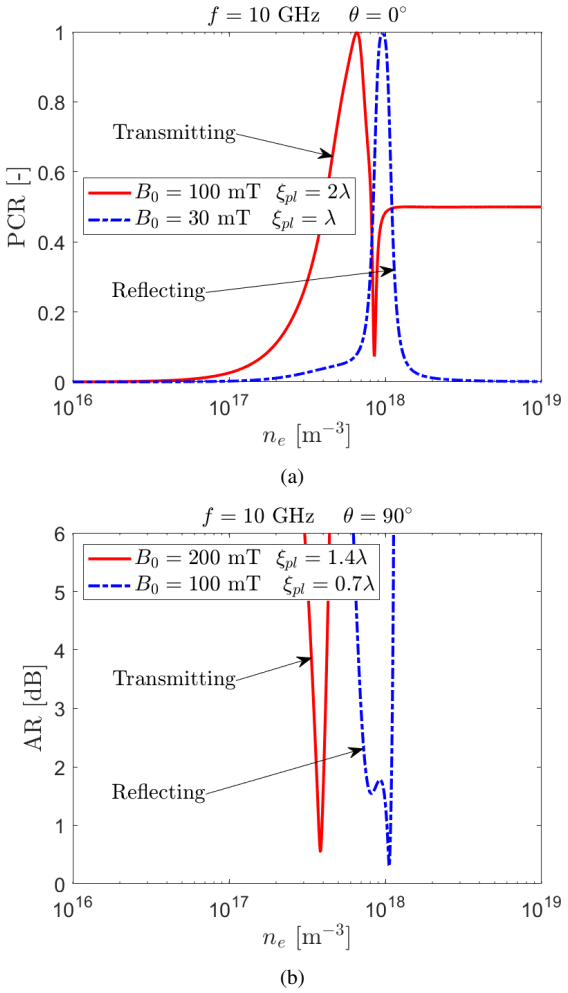

FIGURE 5. Comparison between magnetized transmitting and reflecting surfaces in terms of (a) Polarization Conversion Ratio (PCR), and (b) Axial Ratio (AR), $\nu = 3.1 \times 10^8$ Hz.

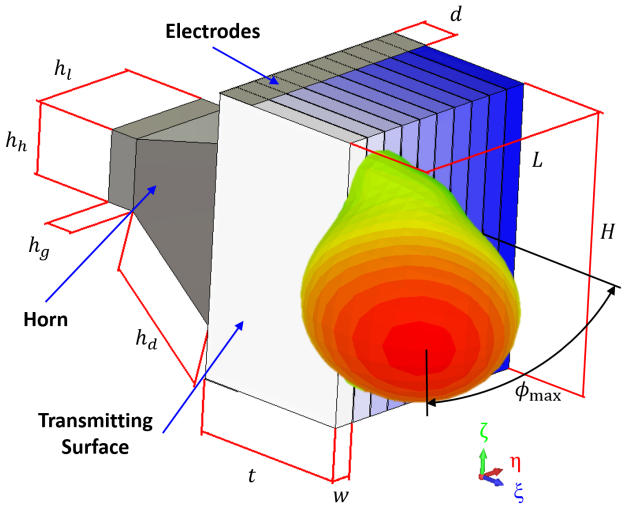

FIGURE 6. Rendering of the plasma-aided horn antenna and radiation pattern for a steering angle of $\phi_{\max} = -50°$. Plasma elements are represented with different colors according to plasma density values reported in Table 1.

TABLE 1. Values of the plasma density in each element N to cause a steering angle of $\phi_{\max} = -50°$. Phase of the transmission coefficient T estimated with the theoretical model.

N [-]	1	2	3	4	5
n_e [10^{17} m^{-3}]	0.1	2.7	4.9	7.0	8.7
ang(T) [deg]	-2	-41	-81	-120	-160
N [-]	6	7	8	9	10
n_e [10^{17} m^{-3}]	9.7	10.7	12.0	15.0	24.1
ang(T) [deg]	161	122	82	43	3

control of the phase of T over 360° ensuring $|T| \approx 1$.

Similar considerations hold if a reflecting surface is meant to implement polarization conversion. In Fig. 5 two arrangements are analyzed to implement cross-polarization and linear to circular polarization (LP-to-CP) conversion, respectively. Consistently with the literature [10], the assumption $\theta = 0°$ is adopted to implement cross-polarization conversion, which is triggered by the Faraday rotation associated with the propagation of R- and L-waves [28]. As proven in Fig. 5(a), the condition PCR $\approx$ 1 is achieved both with transmitting and reflecting surfaces. Nonetheless, the former case requires higher values of both B_0 and ξ_{pl}. LP-to-CP conversion is obtained assuming $\theta = 90°$ [10]. In this case, polarization is controlled by relying on the propagation of O- and X-waves [28]. The condition AR $<$ 3 dB is achieved both for transmitting and reflecting configurations, but the former impose more demanding requirements in terms of B_0 and ξ_{pl} (see Fig. 5(b)).

To sum up, transmitting plasma surfaces are proven to be an appealing solution given that the values of n_e, B_0, and ξ_{pl} identified to implement beam steering and polarization control are consistent with the plasma technology at the state of the art [29]. Clearly, this solution requires a larger value of ξ_{pl} with respect to a plasma reflecting surface [9]–[11] to ensure a propagation path long enough to implement the desired features while maintaining $|T| \approx 1$. Similarly, higher, but still realistic, values of B_0 are needed to exploit polarization conversion.

IV. PLASMA-AIDED HORN ANTENNA

Based on the results presented in section III, a numerical model has been developed for the design of a reconfigurable plasma-aided horn antenna. The latter consists of a plasma-based transmitting surface placed in front of a metallic horn antenna (see Fig. 6). The operation frequency is $f = 10$ GHz, thus the dimensions of the horn antenna are $h_l = 22$ mm, $h_h = 13$ mm, $h_g = 5.6$ mm, $h_d = 31$ mm, $h_s = 2$ mm, $h_L = 42$ mm, $h_H = 33$ mm, and $h_\alpha = 20°$. Regarding the dimensions not reported in Fig. 6, h_s is the thickness of the metal walls of the antenna, h_L and h_H are the en-

velope of the front surface, and h_α is the aperture angle of the horn. Regarding the plasma-based transmitting surface $t = \lambda = 30$ mm, $w = \lambda/7 = 4.3$ mm, $L = 10w = 43$ mm, $H = 12w = 51$ mm, $d = \lambda/4 = 7.5$ mm, and $s = 0.2$ mm. Where s is the thickness of a dielectric vessel that confines each plasma element. The EM response of the dielectric is computed assuming the relative permittivity $\varepsilon_r = 2$, and loss tangent $\tan\delta = 5.4\times10^{-3}$. The signal is fed via a waveguide port placed on the back of the horn antenna. It is worth noting that to enhance the reliability of the proposed design, the electrodes to sustain the discharge and the dielectric vessel to confine the plasma have been included. Moreover, $\nu = 3.1 \times 10^8$ Hz consistently with the plasma technology at the state of the art [29].

A. BEAM STEERING

The proposed design is analysed in terms of beam steering capabilities. The value of n_e in each of the ten plasma elements that constitute the transmitting surface is varied to impose a certain phase profile and, in turn, to tilt the direction of the main lobe in the azimuth plane (ξ–η). A steering angle $\phi_{\max} = -50°$ is achievable assuming n_e according to Table 1. Notably, the prescribed values have been derived by applying the array factor rule [30] to the results of the theoretical model described in section II. Reconfiguring n_e, it is possible to vary $|\phi_{\max}|$ in the range 0°–50° maintaining the gain $>$ 10 dBi, the relative Side Lobe Level (SLL) < -10 dB, the reflection coefficient $|S_{11}| < -10$ dB, and the total radiation efficiency $\eta > 0.85$ (see Fig. 7 and Table 2).

The results obtained regarding beam steering can be analysed according to the theoretical model described in section II. It provides qualitative indications given that some of its hypotheses are not used in the design at hand. For example, the EM field radiated by a horn antenna in the near field is appreciably different from that of a plane wave [30] and, according to the present theoretical formulation, the dielectric vessels that confine the plasma have been neglected. Nevertheless, the theoretical model provides a preliminary estimation of n_e. This is done by selecting the n_e values that produce the phase shift prescribed by the array factor rule to induce a certain steering angle (see Table 1). Moreover, some values of n_e reported in Table 1 exceed $n_e^p \approx 10^{18}$ m^{-3}. This causes an increment of $|S_{11}|$ given the power backscattered by the elements of the transmitting surface where $n_e > n_e^p$. As a result, $|S_{11}|$ increases with $\phi_{\max}$ since larger steering angles require higher values of n_e [9]. This is the main limitation of the steering range since imposing $|\phi_{\max}| > 50°$ causes the increase of the elements in which $n_e > n_e^p$ and, in turn, $|T| < 1$. Thus, the radiation pattern is distorted and steering angles larger than 50° are not achievable with the proposed horn antenna. From a technological standpoint, the maximum value $n_e = 2.41 \times 10^{18}$ m^{-3} is compatible with plasma discharges at the state of the art [29].

The proposed design is further analysed as the operation frequency varies (see Fig. 8 and Table 3). Remarkably, the conditions gain $>$ 10 dBi, SLL < -10 dB, $|S_{11}| < -10$ dB, $\eta > 0.85$, and $\phi_{\max}$ within $\pm1°$ of the nominal value are maintained in the range 9.1–10.1 GHz. This has been obtained for the specific case $\phi_{\max} = -40°$, but comparable results hold for different steering angles. It is worth mentioning that the aperture efficiency η_A of the proposed plasma-aided horn antenna varies in the range $0.65 - 0.8$ following the same trend of the gain [30]. These values are compatible with standard horn antennas [30]. Finally, the bandwidth of the plasma-based systems is generally large compared with more standard solutions [24], [27], consistently with the reflecting surface technology [9]–[11].

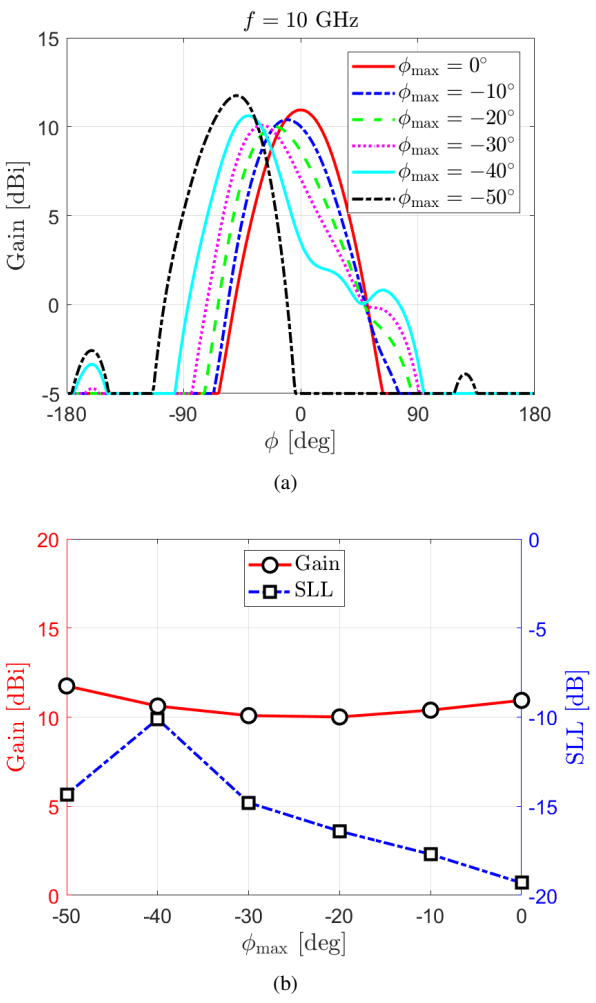

FIGURE 7. Plasma-aided horn antenna: (a) radiation pattern as a function of the azimuth angle ϕ, (b) gain and relative Side Lobe Level (SLL) for different steering angles $\phi_{\max}$.

TABLE 2. Reflection coefficient $|S_{11}|$ and total radiation efficiency η of the plasma-aided horn antenna for different steering angles $\phi_{\max}$, $f = 10$ GHz.

$\phi_{\max}$ [deg]	0	−10	−20	−30	−40	−50
$\lvert S_{11}\rvert$ [dB]	−25.9	−29.3	−24.9	−20.8	−17.1	−10.1
η [-]	0.97	0.96	0.96	0.95	0.94	0.85

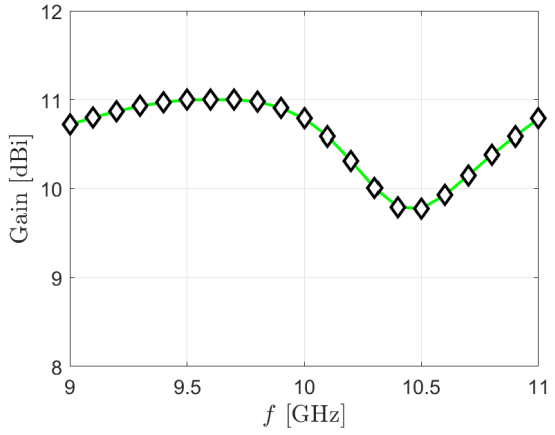

(a)

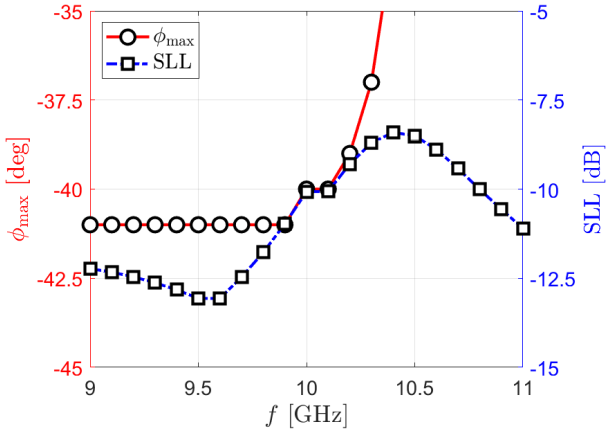

(b)

FIGURE 8. Plasma-aided horn antenna: (a) gain, (b) steering angle $\phi_{\max}$ and relative Side Lobe Level (SLL) as a function of the operation frequency f.

TABLE 3. Reflection coefficient $|S_{11}|$ and total radiation efficiency η of the plasma-aided horn antenna for different frequencies f, $\phi_{\max} = -40°$.

f [GHz]	9	9.5	10	10.5	11
$\lvert S_{11}\rvert$ [dB]	-9.8	-13.5	-17.1	-22.5	-23.9
η [-]	0.87	0.92	0.94	0.95	0.96

B. POLARIZATION CONVERSION

The proposed plasma-aided horn antenna is reconfigurable also in terms of polarization, provided that a suitable induction magnetic field is generated by electromagnets in the nearby. To this end, a uniform value of n_e and B_0 is imposed on all the plasma elements (see Table 4). Cross-polarization conversion can be achieved assuming $\theta = 0°$ [10]. According to Fig. 9, PCR > -1 dB in correspondence of an angle of aperture $\approx 60°$ centered in correspondence of the main lobe. LP-to-CP conversion is feasible too if $\theta = 90°$ [10] and $\psi = 25°$; the latter indicates the angle between $\boldsymbol{B}_0$ and the η-axis. In this case, AR < 3 dB within an angle of aperture

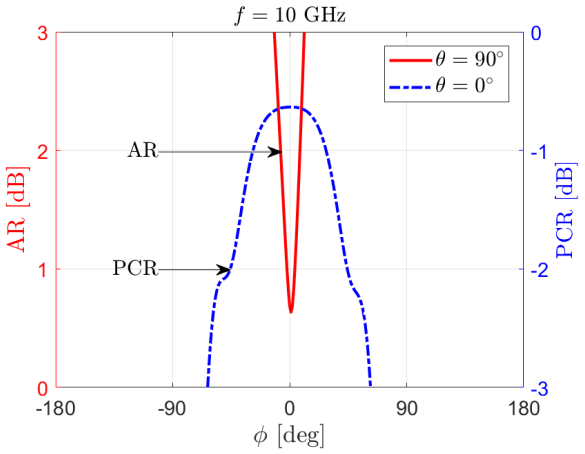

FIGURE 9. Plasma-aided horn antenna: comparison between two magnetized configurations that enable cross-polarization and LP-to-CP conversion. Polarization Conversion Ratio (PCR) and Axial Ratio (AR) in function of the azimuth angle ϕ.

TABLE 4. Parameters of the two configurations that enable cross-polarization and LP-to-CP conversion in the plasma-aided horn antenna, $f = 10$ GHz.

	n_e [m^{-3}]	B_0 [mT]	θ	ψ	Gain [dBi]	$\lvert S_{11}\rvert$ [dB]
LP	4.1×10^{17}	200	0°	–	9.3	-18.2
CP	4.3×10^{17}	200	90°	25°	6.8	-12.8

$\approx 30°$ centered in the broadside direction. Notably, CP is not achieved assuming $\psi = 45°$, as prescribed by the theoretical model (i.e., $\boldsymbol{E}_i$ rotated of 45° with respect to $\boldsymbol{B}_0$ [10], [11]). This result depends on the EM field generated by a horn antenna which, in the near field, is appreciably different from that of a plane wave [30].

The possibility to implement polarization conversion comes at the cost of a gain $<$ 10 dBi, even though the condition $|S_{11}| < -10$ dB is maintained (see Table 4). Consequently, the aperture efficiency decreases to $\eta_A = 0.6 - 0.45$, while $\eta > 0.85$. From a technological standpoint, the values of n_e and B_0 required to implement polarization conversion are feasible at the state of the art [29].

C. SENSITIVITY ANALYSIS

The robustness of the proposed plasma-based horn antenna is assessed via a sensitivity analysis. The effect on the antenna performance of the dielectric vessels' thickness s and relative permittivity ε_r as well as plasma collision frequency ν has been investigated. The performance when the antenna is exploited for LP-to-CP conversion is depicted in Fig. 10. The values $s = 0.2$ mm and $\varepsilon_r = 2$, selected for the design, allow minimizing AR. Specifically, a tolerance of $\pm 50\%$ on both parameters ensures AR < 3 dB. At the same time, increasing the collision frequency above the design value $\nu = 3.1 \times 10^8$ GHz causes a decrease in the gain and degradation of the AR. Nonetheless, AR < 3 dB if

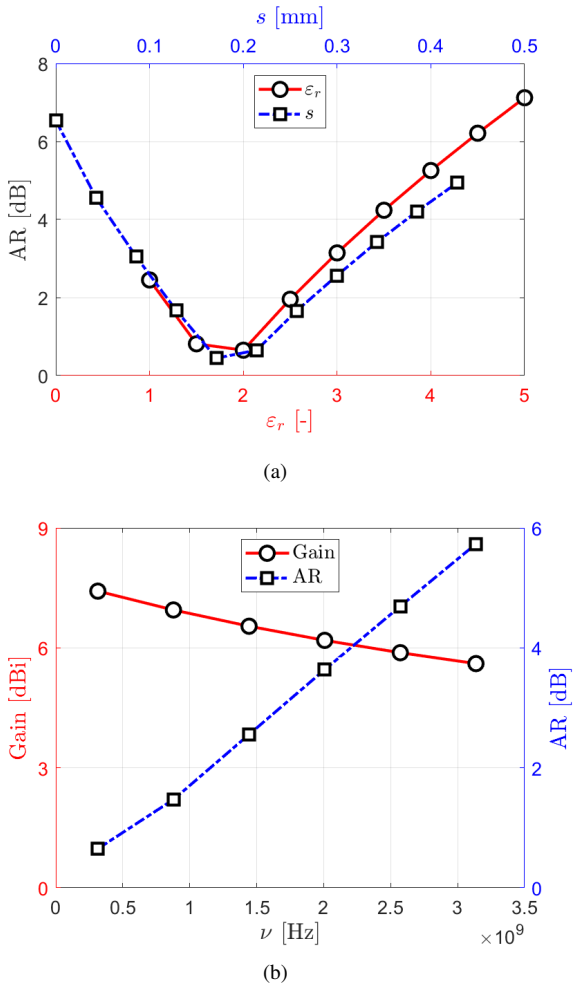

FIGURE 10. Plasma-aided horn antenna: (a) Axial Ratio (AR) in function of the dielectric vessels' thickness s and relative permittivity ε_r, (b) gain and AR in function of the collision frequency ν.

TABLE 5. Gain as a function of the collision frequency ν when the plasma-aided horn antenna is operated to provide $\phi_{\max} = -50°$.

ν [10^8 Hz]	3.1	8.8	14.4	20.1	25.7	31.4
Gain [dBi]	11.8	11.6	11.4	11.2	11.0	10.9

$\nu \approx 1.5 \times 10^8$ GHz, which is 5 times larger than the design value. So, there is a sufficient safety margin in selecting these design parameters.

The AR is the indicator more affected by s, ε_r, and ν. Thus, the operation margins are larger if the plasma-based horn antenna is intended for beam-steering only. For example, increasing ν of one order of magnitude causes a decrease of the gain of $\approx$ 1 dB (see Table 5). At the same time, other performance indicators as $\phi_{\max}$, SLL and $|S_{11}|$ are marginally affected by s, ε_r, and ν. These trends can be explained from a physical standpoint since Ohmic losses occurring within plasma correlate with ν [9]. Instead, s and ε_r can modify reflections occurring at the plasma interfaces with a consequent effect on the transmission coefficient T [9]. This might be studied with an upgraded version of the theoretical model, including the propagation through the dielectric slab [23]. Nonetheless, such an effect seems not critical for the present design, so this upgrade of the theoretical model is left for future work.

V. CONCLUSIONS

A theoretical model that relies on the formalism of the ABCD matrices has been proposed to preliminary design plasma-based reflecting and transmitting surfaces. It has been verified and exploited to prove the feasibility of plasma-based surfaces for beam steering and polarization control. The findings of the theoretical model laid the basis for the design of a reconfigurable plasma-aided horn antenna. The latter relies on a plasma-based transmitting surface placed in front of a metallic horn antenna. The numerical design accounts for practical constraints as the presence of a dielectric vessel that confines the plasma and the interaction between the transmitting surface a realistic EM field. For the first time, the capability to perform both beam steering and polarization control has been demonstrated for a GPA operated in transmission. The possibility to steer the main lobe in the range $0° - 50°$ with a gain > 10 dBi, a relative SLL < -10 dB, $|S_{11}| < -10$ dB, and $\eta > 0.85$ has been proven over a bandwidth of 1 GHz. Moreover, both cross-polarization and LP-to-CP conversion are feasible assuming values of the plasma parameters and magnetic induction field compatible with the technology at the state of the art [29].

The realization and testing of the plasma-aided horn antenna will be the subject of future work. In fact, the proposed design is technologically feasible, but several challenges shall be overcome before its practical implementation. First, the numerical design relies on rectangular plasma elements. One technological solution to implement this design envisions the use of Dielectric Barrier Discharges (DBD), which have been widely employed in the framework of plasma display panels [31]. Nonetheless, advances in terms of electrode design and power consumption are needed for their exploitation in the field of GPAs. It is worth specifying that this is not a killing factor for the technology at hand since, according to recent measures, the assumed values of plasma density and magnetic induction field are feasible with plasma discharges commonly employed for GPAs [11], [12]. Second, the design of the electronics to sustain the plasma shall be optimized and miniaturized according to the solutions recently proposed for space electric propulsion [32], [33]. To conclude, the path toward realizing a reconfigurable plasma-aided horn antenna is challenging but feasible.

AKNOWLEDGEMENTS

This work was partially supported by the European Union under the Italian National Recovery and Resilience Plan (NRRP) of NextGenerationEU, partnership on "Telecom-

munications of the Future" (PE00000001 - program "RESTART").

REFERENCES

[1] T. Anderson, *Plasma antennas*. Artech House, 2020.
[2] G. G. Borg *et al.*, "Plasmas as antennas: Theory, experiment and applications," *Physics of Plasmas*, vol. 7, no. 5, pp. 2198–2202, 2000.
[3] M. Magarotto *et al.*, "Numerical suite for gaseous plasma antennas simulation," *IEEE Transactions on Plasma Science*, vol. 49, no. 1, pp. 285–297, 2020.
[4] M.-R. Dorbin, A. K. Horestani, F. Sadeghikia, M. T. Noghani, and H. Jaafar, "Analytical study on the resonance frequency of tunable surface-wave-excited plasma antennas," *IEEE Transactions on Antennas and Propagation*, vol. 70, no. 10, pp. 9073–9082, 2022.
[5] P. De Carlo *et al.*, "Experimental characterization of a plasma dipole in the uhf band," *IEEE Antennas and Wireless Propagation Letters*, vol. 20, no. 9, pp. 1621–1625, 2021.
[6] F. Sadeghikia, M. Valipour, M. T. Noghani, H. Ja'afar, and A. K. Horestani, "3d beam steering end-fire helical antenna with beamwidth control using plasma reflectors," *IEEE Transactions on Antennas and Propagation*, vol. 69, no. 5, pp. 2507–2512, 2020.
[7] P. De Carlo *et al.*, "Feasibility study of a novel class of plasma antennas for satcom navigation systems," *Acta Astronautica*, vol. 178, pp. 846–853, 2021.
[8] T. Naito, S. Yamaura, Y. Fukuma, and O. Sakai, "Radiation characteristics of input power from surface wave sustained plasma antenna," *Physics of Plasmas*, vol. 23, no. 9, p. 093504, 2016.
[9] M. Magarotto, L. Schenato, P. De Carlo, and A.-D. Capobianco, "Feasibility of a plasma-based intelligent reflective surface," *IEEE Access*, vol. 10, pp. 97 995–98 003, 2022.
[10] ——, "Plasma-based reflective surface for polarization conversion," *IEEE Transactions on Antennas and Propagation*, vol. 71, no. 3, pp. 2849–2854, 2023.
[11] M. Magarotto, L. Schenato, M. Santagiustina, A. Galtarossa, and A.-D. Capobianco, "Plasma-based intelligent reflecting surface for beam-steering and polarisation conversion," *IEEE Access*, vol. 11, pp. 43 546–43 556, 2023.
[12] M. Magarotto *et al.*, "Design of a plasma-based intelligent reflecting surface," *Physics of Plasmas*, vol. 30, no. 4, 2023.
[13] ——, "Feasibility study on a plasma based reflective surface for satcom systems," *Acta Astronautica*, vol. 208, pp. 55–61, 2023.
[14] H. A. E.-A. Malhat, M. M. Badawy, S. H. Zainud-Deen, and K. H. Awadalla, "Dual-mode plasma reflectarray/transmitarray antennas," *IEEE Transactions on Plasma Science*, vol. 43, no. 10, pp. 3582–3589, 2015.
[15] S. H. Zainud-Deen, H. A. E.-A. Malhat, S. M. Gaber, and K. H. Awadalla, "Beam steering plasma reflectarray/transmitarray antennas," *Plasmonics*, vol. 9, pp. 477–483, 2014.
[16] H. A. E.-A. Malhat, M. M. Badawy, S. H. Zainud-Deen, and K. H. Awadalla, "Plasma reflectarray/transmitarray antennas using a single structure," *Plasmonics*, vol. 10, pp. 1479–1487, 2015.
[17] S. H. Zainud-Deen, M. M. Badawy, and H. A. E.-A. Malhat, "Dielectric resonator antenna loaded with reconfigurable plasma metamaterial polarization converter," *Plasmonics*, vol. 14, no. 6, pp. 1321–1328, 2019.
[18] G. Mansutti *et al.*, "Modeling and design of a plasma-based transmit-array with beam scanning capabilities," *Results in Physics*, vol. 16, p. 102923, 2020.
[19] ——, "Design of a hybrid metal-plasma transmit-array with beam-scanning capabilities," *IEEE Transactions on Plasma Science*, vol. 50, no. 3, pp. 662–669, 2022.
[20] F. Sadeghikia, K. Zafari, M.-R. Dorbin, M. Himdi, and A. K. Horestani, "Reconfigurable biconcave lens antenna based on plasma technology," *Scientific Reports*, vol. 13, p. 9213, 2023.
[21] A. B. Petrin, "On the transmission of microwaves through plasma layer," *IEEE Transactions on Plasma Science*, vol. 28, no. 3, pp. 1000–1008, 2000.
[22] ——, "Transmission of microwaves through magnetoactive plasma," *IEEE Transactions on Plasma Science*, vol. 29, no. 3, pp. 471–478, 2001.
[23] D. M. Pozar, *Microwave engineering*. John wiley & sons, 2011.
[24] C. Huang, W. Pan, X. Ma, B. Zhao, J. Cui, and X. Luo, "Using reconfigurable transmitarray to achieve beam-steering and polarization manipulation applications," *IEEE Transactions on Antennas and Propagation*, vol. 63, no. 11, pp. 4801–4810, 2015.
[25] L. Di Palma *et al.*, "Circularly-polarized reconfigurable transmitarray in ka-band with beam scanning and polarization switching capabilities," *IEEE transactions on antennas and propagation*, vol. 65, no. 2, pp. 529–540, 2016.
[26] M. Hwang, G. Kim, J. Kim, and S. Kim, "A simultaneous beam steering and polarization converting s-band transmitarray antenna," *IEEE Access*, vol. 10, pp. 105 111–105 119, 2022.
[27] I.-G. Lee, J.-Y. Kim, and I.-P. Hong, "Design of multi-functional transmitarray with active linear polarization conversion and beam steering capabilities," *Applied Sciences*, vol. 12, no. 9, p. 4319, 2022.
[28] J. A. Bittencourt, *Fundamentals of plasma physics*. Springer Science & Business Media, 2004.
[29] A. Daykin-Iliopoulos *et al.*, "Characterisation of a thermionic plasma source apparatus for high-density gaseous plasma antenna applications," *Plasma Sources Science and Technology*, vol. 29, no. 11, p. 115002, 2020.
[30] C. A. Balanis, *Antenna theory: analysis and design*. John wiley & sons, 2015.
[31] J. Boeuf, "Plasma display panels: physics, recent developments and key issues," *Journal of physics D: Applied physics*, vol. 36, no. 6, p. R53, 2003.
[32] M. Manente *et al.*, "Regulus: A propulsion platform to boost small satellite missions," *Acta Astronautica*, vol. 157, pp. 241–249, 2019.
[33] N. Bellomo *et al.*, "Design and in-orbit demonstration of regulus, an iodine electric propulsion system," *CEAS Space Journal*, vol. 14, no. 1, pp. 79–90, 2022.

MIRKO MAGAROTTO (M'23) received an M. Sc. degree in aerospace engineering and a Ph.D. in science technology and measurements for space from the University of Padova, Padova, Italy, in 2015 and 2019, respectively. He is a Research Fellow (RTDa) with the Dept. of Information Engineering, University of Padova. His current research interests are plasma antennas, plasma numerical simulation, and electric space propulsion.

LUCA SCHENATO (M'06) received an M.Sc. degree in telecommunication engineering and a Ph.D. in electronic and telecommunication engineering from the University of Padova, Padova, Italy, in 2003 and 2007. He is an Assistant Professor (RTDb) with the Dept. of Information Engineering, University of Padova. His research interests include optical fiber sensors, optical fiber-based devices, and intelligent reflective surfaces.

MARCO SANTAGIUSTINA (M'06) received the M.Sc. degree in electronic engineering and the Ph.D. in electronic and telecommunication engineering from the University of Padova, Padova, Italy, in 1992 and 1996, respectively. He is a Full Professor at the Dept. of Information Engineering, University of Padova. His current research interests include nonlinear optics, optical fibers, and electromagnetic field theory.

ANDREA GALTAROSSA (FM'18) is a Full Professor of Electromagnetic Waves and Photonics at the Dept. of Information Engineering, University of Padova, Italy. He has co-authored more than 200 papers in journals and conference proceedings. His research activity is mainly in optical fiber design, distributed characterization of single mode and special fibers, and distributed sensing. He has been the Topical Editor and Deputy Editor for Optics Letters. He has been a member of the Technical Program Committee for the European Conference on Optical Communication (ECOC) and the Optical Fiber Communication Conference (OFC). He is a Fellow of IEEE and OPTICA.

ANTONIO-DANIELE CAPOBIANCO (M'10) received an M.Sc. degree in electronic engineering and a Ph.D. in electronic and telecommunication engineering from the University of Padova, Padova, Italy, in 1989 and 1994, respectively. He is an Associate Professor with the Dept. of Information Engineering, University of Padova. His current research interests include theory and numerical modeling in photonics, plasmonics, and microwave antennas.